

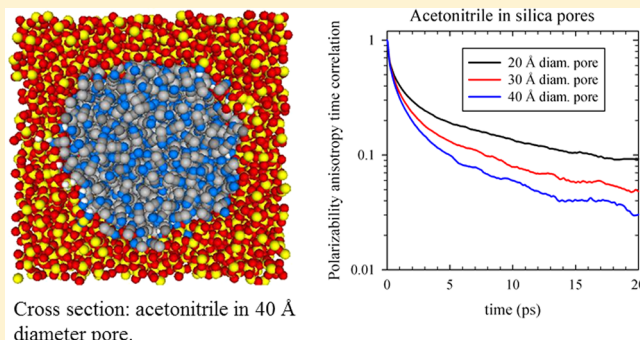
Polarizability Anisotropy Relaxation in Nanoconfinement: Molecular Simulation Study of Acetonitrile in Silica Pores

Anatoli A. Milischuk* and Branka M. Ladanyi*

Department of Chemistry, Colorado State University, Fort Collins, Colorado 80523-1872, United States

Supporting Information

ABSTRACT: We present the results of a molecular simulation study of polarizability anisotropy relaxation of liquid acetonitrile confined in approximately cylindrical silica pores of diameters in the range of 20–40 Å. Grand Canonical Monte Carlo simulation is used to determine the density of acetonitrile in pores in equilibrium with the bulk liquid, and canonical-ensemble molecular dynamics is then used to calculate the trajectories of the filled pores prepared in this way. We find that the pores are wetting, partially due to hydrogen bonding between acetonitrile nitrogen and pore silanol groups and that acetonitrile molecules have preferential orientations relative to the interface. The mobility of molecules in interfacial regions is considerably reduced and dependent mainly on their proximity to the interface. We include the contributions of molecular and interaction-induced polarizabilities to the collective polarizability anisotropy relaxation. We find that this relaxation includes a slowly relaxing component absent from the corresponding process in bulk acetonitrile and that the amplitude of this component increases as the pore diameter decreases. These results are in agreement with optical Kerr effect experiments on acetonitrile in silica pores in a similar diameter range. Further analysis of our data indicates that collective reorientation and predominantly translational “collision-induced” polarizability dynamics both contribute to the slowly relaxing portion of polarizability anisotropy decay. We further find that pore anisotropy plays a role, giving rise to different relaxation rates of polarizability anisotropy components with a different mix of axial and radial character and that collective reorientation contributing to polarizability anisotropy relaxation is somewhat faster at long times than single-molecule orientational relaxation.



1. INTRODUCTION

The dynamics of liquids in nanoscopic pores is of considerable interest from scientific and technological points of view. Among the scientific issues that arise is the impact of molecular-scale surface roughness, interactions within interfacial layers, and the effects of confinement size and geometry on the observable liquid dynamics. Answers to these questions have implications for the technological applications of nanoporous materials in areas such as separations, nanofluidics, and catalysis.

Among the experimental methods used in the studies of dynamics of confined fluids, optical Kerr effect (OKE) has played an important role in recent years.^{1–12} OKE is a pump–probe technique that detects the relaxation of the transient refractive index anisotropy created by a pump pulse.^{13,14} The response consists of an essentially instantaneous electronic component and the nuclear component that arises from the relaxation of the collective polarizability anisotropy of the liquid sample.^{15,16} It is the nuclear response that contains dynamical information about the confined fluid.¹

Most of the OKE experiments on confined fluids have been carried out using silica materials with approximately cylindrical pore structure.¹ Silica surfaces are partially hydroxylated^{17,18} under ambient conditions, and their wettability can be tuned by

chemical modification.^{19,20} OKE response of liquids in wetting pores exhibits nonexponential decay, which resembles in some respects the response observed for bulk supercooled liquids.^{21,22}

In the present case, our focus is on acetonitrile in approximately cylindrical silica pores in the diameter range characteristic of MCM-41 materials.²³ Acetonitrile in such nanopores has been studied by OKE,^{3,12} with the results exhibiting strong dependence on the pore diameter.

Several MD studies have focused on the properties of acetonitrile in silica pores.^{24–26} They have characterized the interfacial structure,^{24,25} including density profiles and molecular alignment relative to the pore surface as well as single-molecule translational and rotational mobility in interfacial layers.^{25,26} Polarizability anisotropy, which contributes to OKE nuclear response, is a collective variable, and its characterization will therefore provide new information on the molecular origin of the dynamics of confined acetonitrile. It should be noted that polarizability anisotropy relaxation in bulk liquid acetonitrile

Special Issue: Michael D. Fayer Festschrift

Received: June 30, 2013

Revised: September 5, 2013

Published: September 5, 2013

trile^{27–30} and in a liquid acetonitrile film on a flat silica surface³¹ have been studied by MD, and it will be instructive to determine the origin of the differences among the OKE responses of bulk, interfacial, and nanoconfined liquids.

The remainder of this article is organized as follows: Section 2 includes the theoretical background for the polarizability model and the OKE response used in our calculations. It also describes the interaction models and simulation procedures for the silica–acetonitrile system. In Section 3, we start by presenting some MD results on interfacial structure and single-molecule dynamics of acetonitrile in cylindrical silica pores in the diameter range 20–40 Å, followed by the MD results on the polarizability anisotropy relaxation. The nanopore results are compared with those for bulk acetonitrile. In both cases, the contributions of molecular and interaction-induced polarizability are determined and the roles of the contributing molecular mechanisms investigated. MD results for the polarizability anisotropy time correlation are used to calculate the OKE nuclear response, which is compared with experiment. Our main results are summarized and the article is concluded in Section 4.

2. MODEL AND SIMULATION DETAILS

2.A. Polarizability Anisotropy Relaxation. The collective polarizability of a fluid sample is a sum of molecular (M) and interaction-induced (I) terms^{32–34}

$$\Pi = \Pi^M + \Pi^I \quad (1)$$

where Π^M is a sum of polarizabilities α_i of individual molecules:

$$\Pi^M = \sum_{i=1}^N \alpha_i \quad (2)$$

Π^I arises from interactions between molecular induced dipoles. In the case of liquid acetonitrile, a reasonable representation of Π^I is obtained by assuming that the interaction is between ideal induced dipoles located at the molecular centers-of-mass and that only the leading order in these interactions contributes significantly.²⁹ This leads to:^{33,35}

$$\Pi^I \cong \sum_{i=1}^N \sum_{j \neq i} \alpha_i \cdot \mathbf{T}(\mathbf{r}_{ij}) \cdot \alpha_j \quad (3)$$

where \mathbf{T} is the dipole tensor:

$$\mathbf{T}(\mathbf{r}) = \frac{3\hat{\mathbf{r}}\hat{\mathbf{r}} - \mathbf{1}}{4\pi\epsilon_0 r^3} \quad (4)$$

$\hat{\mathbf{r}} = \mathbf{r}/r$ is a unit vector along \mathbf{r} and $\mathbf{1}$ is a unit tensor.

In bulk liquid, the time-correlation function (TCF) that represents polarizability anisotropy relaxation can be calculated from any off-diagonal element of Π ,³⁶ for example, Π_{xz} :

$$\Psi(t) = \frac{\langle \Pi_{xz}(0)\Pi_{xz}(t) \rangle}{N\gamma^2/15} \quad (5)$$

where γ is the molecular polarizability anisotropy. For an axially symmetric molecule such as acetonitrile, the molecular polarizability has components $\alpha_{||}$ and α_{\perp} that are, respectively, parallel and perpendicular to the molecular symmetry axis. Thus the polarizability of molecule i is

$$\alpha_i = \alpha_0 \mathbf{1} + \gamma \mathbf{Q}_i \quad (6)$$

where

$$\mathbf{Q}_i = \left(\hat{\mathbf{u}}_i \hat{\mathbf{u}}_i - \frac{1}{3} \mathbf{1} \right) \quad (7)$$

$\hat{\mathbf{u}}_i$ is a unit vector along the molecular symmetry axis, the isotropic polarizability is given by

$$\alpha_0 = (\alpha_{||} + 2\alpha_{\perp})/3 \quad (8)$$

and the anisotropy is given by

$$\gamma = \alpha_{||} - \alpha_{\perp} \quad (9)$$

In a liquid confined in a cylindrical pore, the cylinder axis defines a unique direction. If this direction represents the z axis, then relaxation rates for the xz and yz polarizability components might be expected to differ from the relaxation rate of the xy component. In our calculations, we have chosen to present the result for Ψ that is an average over all three off-diagonal components, given that the experimental results sample essentially all pore orientations. We also present a few results in which the polarizability TCF for the average over xz and yz components is compared with the TCF for the xy component.

Given that the polarizability is a sum of molecular and interaction-induced terms according to eq 1, the polarizability anisotropy TCF is a sum of three terms:

$$\Psi(t) = \Psi^{MM}(t) + \Psi^{II}(t) + \Psi^{MI}(t) \quad (10)$$

where the three-component TCFs are given by:

$$\Psi^{MM}(t) = \frac{\langle \Pi_{xz}^M(0)\Pi_{xz}^M(t) \rangle}{N\gamma^2/15} \quad (11)$$

$$\Psi^{II}(t) = \frac{\langle \Pi_{xz}^I(0)\Pi_{xz}^I(t) \rangle}{N\gamma^2/15} \quad (12)$$

and

$$\Psi^{MI}(t) = \frac{\langle \Pi_{xz}^M(0)\Pi_{xz}^I(t) \rangle + \langle \Pi_{xz}^I(0)\Pi_{xz}^M(t) \rangle}{N\gamma^2/15} \quad (13)$$

The polarizability anisotropy TCF can be cast into a projected representation,^{33–35} in which the portion of Π_{xz}^I that relaxes via the same collective reorientation mechanism as Π_{xz}^M is identified. The remainder, the “collision-induced” polarizability anisotropy is given by

$$\Delta\Pi_{xz} = \Pi_{xz}^I - G_{xz}\Pi_{xz}^M \quad (14)$$

where

$$G_{xz} = \frac{\langle \Pi_{xz}^M(0)\Pi_{xz}^I(0) \rangle}{\langle |\Pi_{xz}^M|^2 \rangle} = \frac{\Psi^{MI}(0)}{2\Psi^{MM}(0)} \quad (15)$$

(1 + G_{xz}) acts as a local field factor for the molecular polarizability anisotropy³⁷ by providing the scaling due to the local environment and by identifying Π_{xz}^R , the part of Π_{xz} that relaxes via collective reorientation:

$$\Pi_{xz}^R = (1 + G_{xz})\Pi_{xz}^M \quad (16)$$

The total polarizability anisotropy can now be expressed as

$$\Pi_{xz} = \Pi_{xz}^R + \Delta\Pi_{xz} \quad (17)$$

and its TCF is

$$\Psi(t) = \Psi^{RR}(t) + \Psi^{AD}(t) + \Psi^{RD}(t) \quad (18)$$

with the components

$$\Psi^{RR}(t) = \frac{\langle \Pi_{xz}^R(0)\Pi_{xz}^R(t) \rangle}{N\gamma^2/15} = (1 + G_{xz})^2 \Psi^{MM}(t) \quad (19)$$

$$\Psi^{\Delta\Delta}(t) = \frac{\langle \Delta\Pi_{xz}(0)\Delta\Pi_{xz}(t) \rangle}{N\gamma^2/15} \quad (20)$$

and

$$\Psi^{R\Delta}(t) = \frac{\langle \Pi_{xz}^R(0)\Delta\Pi_{xz}(t) \rangle + \langle \Pi_{xz}^R(t)\Delta\Pi_{xz}(0) \rangle}{N\gamma^2/15} \quad (21)$$

Note that this projection scheme leads to initial lack of cross-correlation between rotational and collision-induced components: $\Psi^{R\Delta}(0) = 0$.

The connection between $\Psi(t)$ and OKE experiments can be obtained by calculating the nuclear response function:^{15,16}

$$R^{\text{nuc}}(t) = -\frac{\Theta(t)}{k_B T} \frac{\partial \Psi(t)}{\partial t} \quad (22)$$

where $\Theta(t)$ is the Heaviside step function.

2.B. Interaction Model and Simulation Details. Our simulations of acetonitrile in silica pores proceed by first constructing the pores, then filling them with acetonitrile in equilibrium with the bulk liquid and then carrying out MD simulations of confined acetonitrile. The procedure that we use for constructing the pores in amorphous silica has been developed by Gulmen and Thompson.^{38,39} In our systems, a single pore is constructed along the z axis in the center of the xy face of a silica sample.^{40,41} The sample has orthorhombic shape with outer dimensions $L_z = 40 \text{ \AA}$ and $L_x = L_y = 60 \text{ \AA}$.⁴¹ Hydroxyl hydrogens are added to the reactive surface oxygens, identified using the criteria developed by Gulmen and Thompson.³⁸ The numbers of the resulting surface OH groups are listed in Table 1.

Table 1. Numbers of Acetonitrile Molecules and Surface Hydroxyl Groups in Silica Pores

diameter/\text{\AA}	N_{acn}	N_{OH}
20	225	64
30	432	96
40	723	104

The atoms in the silica pore are treated as stationary in simulations of the silica–acetonitrile systems. The filling of the pores is carried out by a Grand Canonical Monte Carlo algorithm using the MCCS Towhee suite of programs.^{42,43} The pores are considered to be filled when equilibrium with the bulk liquid under ambient conditions (300 K, 1 bar) has been reached. The resulting numbers of molecules are listed in Table 1. MD simulations are then performed on the filled pores, using the DL_POLY Classic simulation package.⁴⁴ The simulations were performed in the NVT ensemble, using the Nosé–Hoover thermostat.^{45–47} The particle-mesh Ewald sum method⁴⁸ was used for the long-ranged Coulomb interactions. After equilibration, production runs of at least 20 ns were used in the calculations of the collective TCFs. We have also carried out for comparison a simulation of bulk acetonitrile, using a 256 molecule sample at the same temperature and pressure as the confined acetonitrile.

Acetonitrile (CH_3CN) molecules are represented as rigid objects containing three interaction sites; that is, the methyl group, CH_3 , is represented as a single site, Me. Intermolecular interactions and interactions of acetonitrile with the silica pore

atoms are represented as Lennard-Jones (LJ) + Coulomb site–site potentials. Lorentz–Berthelot combining rules⁴⁹ are used to construct LJ interaction parameters for unlike site pairs. We are using the ANL potential,⁵⁰ developed by Gee and van Gunsteren, for acetonitrile. These parameters are listed in Table 2. As in our previous work,^{40,41} we are using for silica the Bródka–Zerda LJ parameters⁵¹ and Gulmen–Thompson partial charges.³⁹

Table 2. Acetonitrile Potential Parameters

site	q/e	$\epsilon/(kJ/mol)$	$\sigma/\text{\AA}$
Me	0.287	1.336	3.48
C	0.1376	0.35	3.287
N	-0.4246	0.35	3.19

A snapshot of the cross-section of the 40 Å diameter pore filled with liquid acetonitrile is shown in Figure 1. As can be seen from the Figure, the pore surface is rough, and the cross section is only approximately circular.

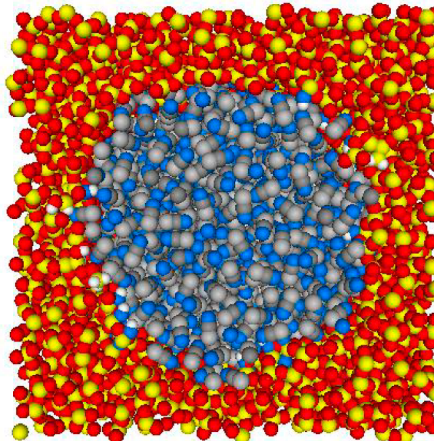


Figure 1. Snapshot of a cross section of the 40 Å diameter silica (red, O; yellow, Si; white, H) pore filled with acetonitrile (light gray, Me; darker gray, C; blue, N).

In the calculation of acetonitrile polarizability anisotropy relaxation, we use the following experimental values⁵² of the molecular polarizability components (in volume units): $\alpha_{||} = 5.80 \text{ \AA}^3$ and $\alpha_{\perp} = 3.65 \text{ \AA}^3$.

3. RESULTS

3.A. Structural Properties and Single-Molecule Dynamics. We first present a few structural properties of acetonitrile in silica pores. Figure 2 depicts radial density profiles for the three pore sizes. As can be seen from the Figure, density is enhanced in the vicinity of the pore surface, indicating that there is attraction between the pore walls and acetonitrile molecules. In the largest diameter pore, the density levels off away from the interface, reaching the value that corresponds to the density of the bulk liquid.⁵⁰ In the two smaller pores, the density does not level off and attains a somewhat lower than bulk value in the center of the pore. This behavior is characteristic of a liquid confined in a wetting nanopore.⁵³

It has been observed in previous simulations that acetonitrile molecules adopt a preferential orientation relative to the pore surface^{24,25} and that this preference is related to the surface charge distribution. Because of the interface curvature and roughness, these orientational preferences are less clear-cut than

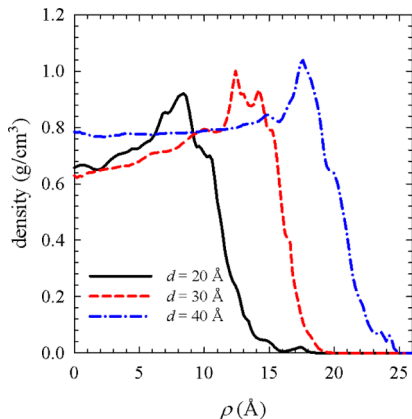


Figure 2. Radial density profiles for the center-of-mass of acetonitrile molecules. Shown are results for three pore sizes with diameters 20, 30, and 40 Å.

in the case of acetonitrile next to a flat crystalline silica surface.^{31,54} Consistent with the flat surface results, they show a preference of the N end of the CH₃CN molecule to point toward the interface in the closest interfacial layer. This orientational preference is illustrated in Figure 3, where the acetonitrile density is plotted against radial distance ρ and the angle θ_n , where

$$\cos \theta_n = \hat{\mathbf{n}} \cdot \hat{\boldsymbol{\mu}} \quad (23)$$

while $\hat{\mathbf{n}}$ and $\hat{\boldsymbol{\mu}}$ are, respectively, unit vectors along the inwardly directed surface normal and the molecular dipole.

As can be seen from the Figure, the density for $\rho > 15$ Å peaks at small θ_n , with the peak shifting to larger values as ρ decreases. At ρ smaller than ~8 Å, the density profile shows no angular preference.

The angular–radial density profile does not vary smoothly with θ and ρ as a consequence of surface roughness, illustrated in Figure 1. Thus a given value of ρ , which is measured from the approximate pore center, represents a range of distances from the interface. Additional information on interfacial structure can be

obtained from pair distributions, corrected for the excluded volume effect of the pore geometry,⁵⁵ connecting silica and acetonitrile sites.

Figure 4 illustrates the pair correlations between the surface silanol groups and the positive (Me) and negative (N) end sites

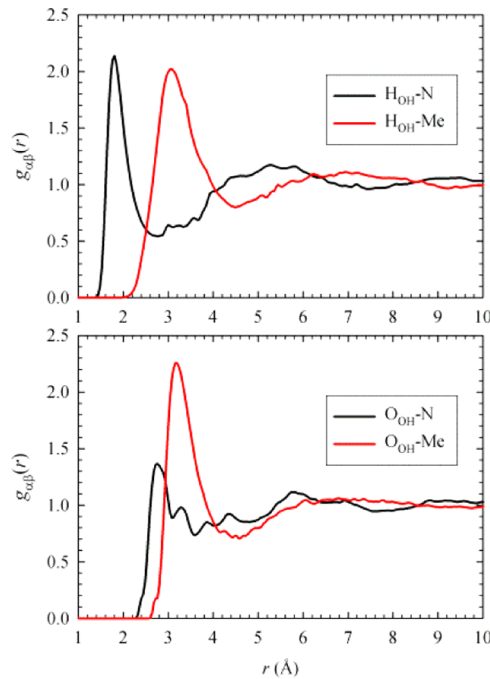


Figure 4. Pair distributions between the surface hydroxyl groups and the acetonitrile N and Me sites in a 40 Å diameter silica pore.

of the acetonitrile molecule. The short NH separation indicates the presence of surface O–H···N hydrogen bonds and can partially account for the orientational preference that we observe. However, previous work has shown that this preference remains even when the hydroxyl H is not included as a separate site, and its charge is added to that of the oxygen of the OH group.²⁶

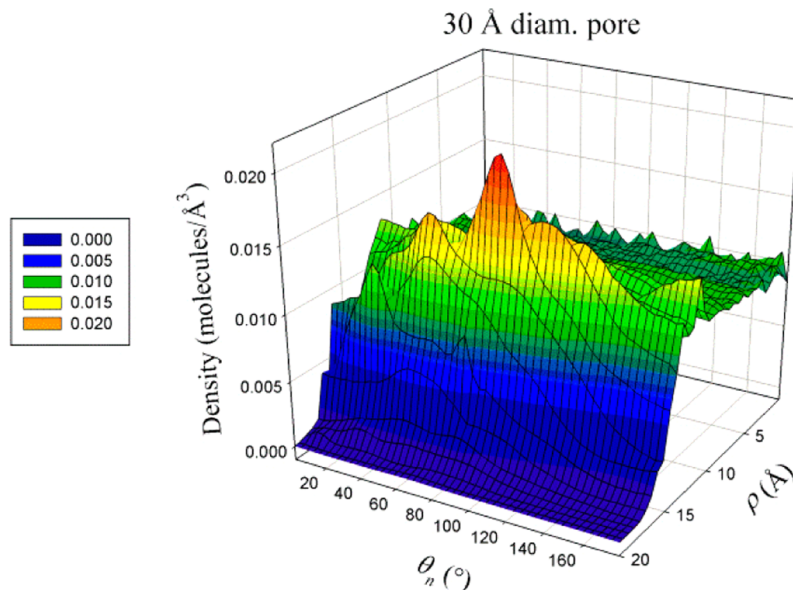


Figure 3. Angular–radial density profile of acetonitrile in the 30 Å diameter pore. The radial coordinate ρ connects the molecular center-of-mass and pore center. The angle is between the molecular dipole and the inwardly directed surface normal.

Collective polarizability anisotropy TCF relaxes through molecular rotations and translations. To understand its behavior in silica pores, it is helpful to consider first simpler measures of these relaxation processes. We do this by calculating molecular mean-squared displacements (MSDs) and single-molecule orientational TCFs. In an approximately cylindrical pore, translational mobility is restricted in the axial, but not in the radial direction.⁵⁶ Proximity to an attractive (wetting) surface also restricts the mobility of molecules in the vicinity of the interface,^{57,58} including acetonitrile–silica interfaces.^{25,31} We examine here how both of these effects manifest themselves in the present systems.

To examine the effects of proximity to the interface on molecular mobility, we divide the pore into three regions along the radial coordinate ρ :⁴¹ For a pore of nominal diameter d , the “outer” region corresponds to $\rho > d/2$, the “surface” region corresponds to $d/2 - 5 \text{ \AA} < \rho \leq d/2$, and the “core” region corresponds to $\rho \leq d/2 - 5 \text{ \AA}$. The molecules are tagged according to their location at $t = 0$ and then followed, regardless of their subsequent location.

The result of this analysis for acetonitrile MSD is shown in Figure 5. As can be seen from the figure, the MSDs in the two

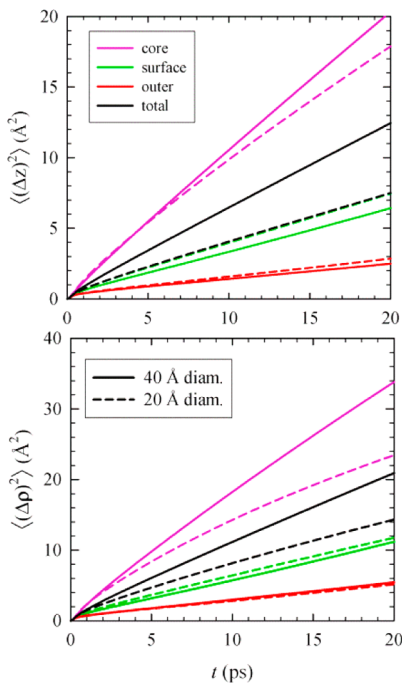


Figure 5. Molecular mean-squared displacements (MSDs) in the axial (top) and radial (bottom) directions for acetonitrile in 20 (dashed line) and 40 Å (full line) diameter pores. Shown are MSDs for molecules initially in the three radial regions (outer, surface, and core). Note that the total and surface region axial MSDs are almost coincident for the 20 Å diameter pore.

regions close to the interface (outer and surface) are weakly dependent on the pore diameter, while a stronger dependence is seen for molecules in the core region. In the smaller-diameter pore, this region has a considerably smaller volume, and most molecules in it do not remain there throughout the 0–20 ps time interval displayed, exhibiting a pronounced slow-down compared to the core-region molecules in the 40 Å diameter pore. This slowdown is more pronounced for the radial MSDs. Translational mobility in axial and radial directions slows down

considerably in interfacial regions, with the result that pore-averaged MSDs are considerably lower in the 20 Å diameter pore than in the 40 Å diameter pore.

To clarify further the issue of molecular mobility in different interfacial layers, we calculate the survival TCFs $S(t)$, which measure the probability that a molecule remains continuously in a given region over the time interval t . We calculate $S(t)$ using the expression given by Liu et al.⁵⁹ We had previously reported $S(t)$ values for water in the same model silica pores.⁴⁰

The results for $S(t)$ in 20 and 40 Å diameter pores are shown in Figure 6. As can be seen from this Figure, molecular mobility as

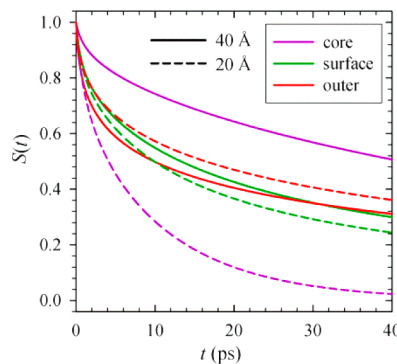


Figure 6. Survival TCFs $S(t)$ for acetonitrile molecules in the three regions (core, surface, and outer) of a 20 Å diameter (dashed line) and 40 Å diameter (full line) pore.

well as the region volume contribute to the decay rate of $S(t)$. The effects of the region size are especially striking for the core region, which has a nine times larger volume in the 40 Å pore than in the 20 Å pore. As a result, $S(t)$ in this region decays much more slowly in the larger pore. In the case of the surface and outer regions, which have the same thickness but different curvatures in the two pores, the differences in the decay rates of $S(t)$ are more modest. Similar results for $S(t)$ for acetonitrile in silica pores have been obtained in previous work.²⁵

We consider the orientational TCF corresponding to the second rank Legendre polynomial of the orientation of the molecular symmetry axis:

$$C_2(t) = \langle P_2[\hat{\mathbf{u}}_i(0) \cdot \hat{\mathbf{u}}_i(t)] \rangle \quad (24)$$

$C_2(t)$ is related to the single-molecule portion of the molecular polarizability anisotropy TCF; that is, it can be written as

$$C_2(t) = \frac{3}{2N} \sum_{i=1}^N \langle \mathbf{Q}_i(0) : \mathbf{Q}_i(t) \rangle \quad (25)$$

where \mathbf{Q}_i is given by eq 7.

The results for $C_2(t)$ for acetonitrile bulk and confined liquids are shown in Figure 7. As can be seen from the results in the top panel, the pore and bulk liquid results decay at similar rates at short times. At longer times, $C_2(t)$ in the bulk remains a single exponential, while in the pores it exhibits nonexponential decay. The slowly decaying long-time portion has larger amplitude in smaller pores, but its decay rate is similar in all three pores. The results shown in the bottom panel, where $C_2(t)$ in different radial regions of 20 and 40 Å diameter pores are compared, illustrate that this slow decay originates from molecules in the layers close to the interface. The rotational relaxation of molecules in the outer and surface regions exhibits nonexponential decay that depends weakly on the pore diameter but is considerably slower

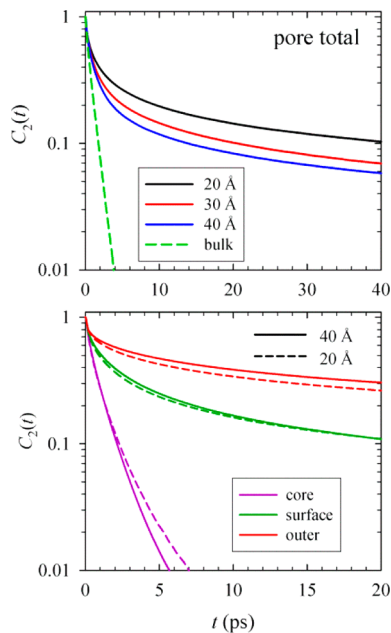


Figure 7. Orientational TCF $C_2(t)$ for acetonitrile. The top panel depicts the results for the bulk liquid and pore-averaged results for the 20, 30, and 40 Å diameter pores. The bottom panel depicts a comparison of the results for molecules initially in three radial regions (outer, surface and core) in 20 (dashed lines) and 40 Å (full lines) diameter pores.

than in the core region. Attraction to the pore surface, pore roughness, and reduced hydrodynamic volume available to rotation are all likely responsible for this behavior.^{1,4,60} We should note that single-molecule orientational relaxation of acetonitrile in silica pores has been previously investigated by MD simulations^{25,26} and similarly slow dynamics of molecules in interfacial layers has been found.

In tagging molecules in different interfacial regions, we have considered molecules that are present there at $t = 0$ but that may have left the region at a later time. One can alternatively consider molecules that remain in a given region over the entire time interval.^{25,59} At short times, the two methods produce similar relaxation rates, but differences occur at longer times, governed by the behavior of the respective $S(t)$ values.^{25,61} We have focused here on molecules that are initially in a given region because this measure is more closely related to their local mobility on short to moderate time scales⁶² but have included our results for continuous residence MSD and $C_2(t)$ values for the 20 and 40 Å diameter pores in the Supporting Information.

3.B. Polarizability Anisotropy Relaxation. Our main results, illustrating the decay of the polarizability anisotropy TCF $\Psi(t)$ of acetonitrile in the pores of different diameter compared with its decay in bulk liquid, are shown in Figure 8.

As can be seen from the Figure, $\Psi(t)$ for bulk acetonitrile decays approximately exponentially, reaching 0.01 of its initial value in <4 ps. At short times the polarizability anisotropy TCFs for acetonitrile decay at a rate similar to the bulk but then depart from it, exhibiting a slowly decaying component. The amplitude of this component increases with decreasing pore diameter, indicating that the slowdown is associated with relaxation of molecules close to the interface. Our results exhibit the same trends with silica pore diameter as were observed in OKE experiments on confined acetonitrile.^{3,12} This trend is also similar to that for the single-molecule orientational TCFs shown in Figure 7.

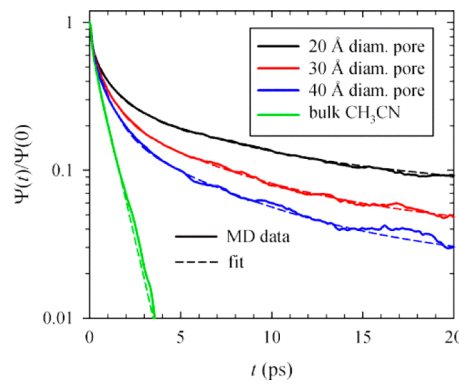


Figure 8. Polarizability anisotropy TCF $\Psi(t)$ for acetonitrile in silica pores of diameters in the range 20–40 Å and in the bulk liquid. Full lines are MD data and dashed lines represent fits to a Gaussian and sums of exponentials.

In anticipation of comparison of the OKE nuclear response to experiment, we have fit our results for $\Psi(t)/\Psi(0)$ using an approach similar to that used in fitting the experimental OKE data.^{3,12} Specifically, we have assumed that the short-time behavior is the same in bulk and confined acetonitrile and that two additional exponential decay mechanisms, characterized by relaxation times independent of pore size, contribute to longer-time decay of $\Psi(t)$ in the pores. Further details and fitting parameters are included in the Supporting Information. As can be seen from Figure 8, the fits provide a good representation of the data over the entire time interval displayed.

The main reason why $\Psi(t)$ is more noisy than $C_2(t)$, displayed in Figure 7, is that it is a collective rather than a single-molecule TCF so that its accuracy cannot be improved by averaging over molecules. While single-molecule orientational relaxation contributes to $\Psi(t)$, it accounts for only a part of the relevant relaxation mechanisms, given that collective reorientation and translational dynamics associated with the interaction-induced polarizability contribute to $\Psi(t)$.

Decomposition of $\Psi(t)$ into its components arising from auto- and cross-correlations of molecular and interaction-induced polarizabilities, shown in eq 10, can provide some insight into the contributing relaxation mechanisms. The results of this decomposition for the bulk liquid and for acetonitrile in a 30 Å diameter pore are shown in Figure 9.

As can be seen from the Figure, the components due to the presence of the interaction-induced polarizability, $\Psi^{\text{MI}}(t)$ and $\Psi^{\text{II}}(t)$, are of the same order of magnitude as the molecular component $\Psi^{\text{MM}}(t)$ in bulk and confined acetonitrile. This indicates that in both cases processes that involve the relaxation of the anisotropic portion of Π^{I} make a significant contribution. To gauge to what extent these processes are dynamically distinct from collective reorientation that governs the relaxation of Π^{M} anisotropy, we carry out the projection of off-diagonal components of Π^{I} along and orthogonal to Π^{M} , as specified in eqs 17–21.

The results of this procedure are illustrated in Figure 10, again for the bulk liquid and for acetonitrile in a 30 Å diameter pore. As can be seen from the Figure, the projection scheme is quite successful in decoupling the rotational relaxation component of $\Psi(t)$, $\Psi^{\text{RR}}(t)$, from $\Psi^{\Delta\Delta}(t)$, the “collision induced” polarizability anisotropy autocorrelation. The cross-correlation $\Psi^{\text{RA}}(t)$ between these polarizability components, defined to vanish at $t = 0$ (see eq 14), remains small at all times. This is true for bulk and confined acetonitrile. Note that because $\Psi^{\text{MI}}(0) < 0$ the

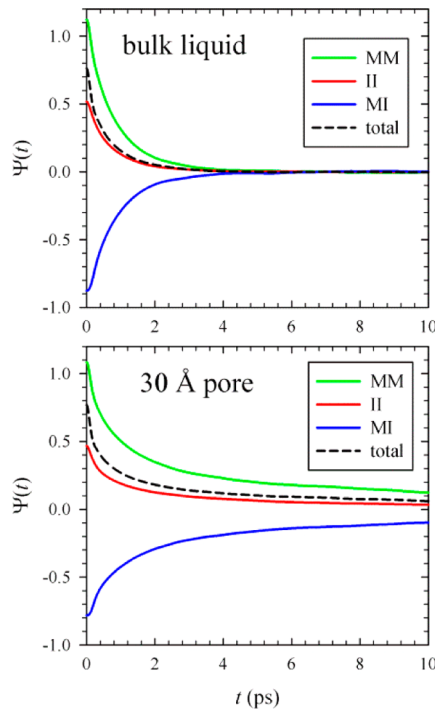


Figure 9. Polarizability anisotropy TCF of bulk liquid (top) and acetonitrile confined in a 30 Å diameter silica pore (bottom). In addition to the total TCF $\Psi(t)$, its components $\Psi^{\text{MM}}(t)$, $\Psi^{\text{MI}}(t)$, and $\Psi^{\text{II}}(t)$ are shown.

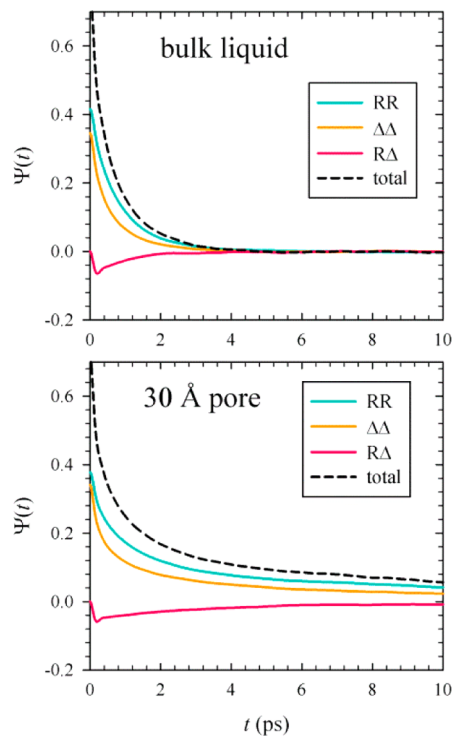


Figure 10. Anisotropy TCF of bulk liquid (top) and acetonitrile confined in a 30 Å diameter silica pore (bottom). In addition to the total TCF $\Psi(t)$, its components in the projected representation, $\Psi^{\text{RR}}(t)$, $\Psi^{\text{RΔ}}(t)$, and $\Psi^{\Delta\Delta}(t)$, are shown.

projection $G_{xz} < 0$, which means that the local field factor $(1 + G_{xz})^2$ decreases the magnitude of the rotational relaxation contribution to $\Psi(t)$ below the value of $\Psi^{\text{MM}}(t)$.

To determine how the relaxation of $\Psi^{\text{RR}}(t)$ and $\Psi^{\Delta\Delta}(t)$ contributes to the relaxation of $\Psi(t)$ in the silica pores, we display these results for the three pore sizes in Figure 11.

As can be seen from this Figure, at short times the collision-induced component, $\Psi^{\Delta\Delta}(t)$, relaxes faster than the rotational relaxation component, $\Psi^{\text{RR}}(t)$, for all three pore sizes. It also relaxes somewhat faster than $\Psi^{\text{RR}}(t)$ at longer times in the 30 and 40 Å diameter pores but not in the narrowest pore, where its long-time relaxation rate is slightly slower. The long-time relaxation rates of $\Psi^{\text{RR}}(t)$ and $\Psi^{\Delta\Delta}(t)$ in a given pore are fairly similar and, while the amplitude of $\Psi^{\text{RR}}(t)$ is somewhat larger than that of $\Psi^{\Delta\Delta}(t)$, both contribute significantly to $\Psi(t)$ over the whole 0–8 ps time interval displayed. Thus we may conclude that $\Psi(t)$ does not have a simple molecular origin but that acetonitrile interactions with the wetting surface act in a similar way on rotational and translational dynamics, contributing to $\Psi(t)$ relaxation.

The TCF results shown so far have been for the average over xy , xz , and yz components of the collective polarizability. In cylindrical pores, molecular translational motion is confined in the radial but not in the axial direction. Rotational motion is impeded due to restricted hydrodynamic volume⁶³ in the interfacial layers, and, as was illustrated in Figures 3 and 4, molecules have a nonuniform orientational distribution close to the silica surface. Thus we expect that pore anisotropy will have an effect on $\Psi(t)$ relaxation. We examine this by comparing the relaxation rates of off-diagonal components of the polarizability tensor in the frame in which the pore axis is along z . In this frame, the xz and yz components are equivalent, while the xy component is purely radial and thus different from these two. This comparison for acetonitrile in a 30 Å diameter pore is illustrated in Figure 12.

These results show strong effects of pore anisotropy on rotational and collision-induced relaxation contributing to $\Psi(t)$. In the case of the axial–radial component, $\Psi_{a-\rho}(t) = [\Psi_{xz}(t) + \Psi_{yz}(t)]/2$, $\Psi_{a-\rho}^{\text{RR}}(t)$ has a larger amplitude and a slower decay rate than $\Psi_{a-\rho}^{\Delta\Delta}(t)$, while for the radial component $\Psi_{xy}(t)$, $\Psi_{xy}^{\Delta\Delta}(t)$ has a larger amplitude and a slower relaxation rate than $\Psi_{xy}^{\text{RR}}(t)$. The pore anisotropy effects on the relaxation of the $\Delta\Delta$ component of the polarizability anisotropy TCF are quite large, suggesting that confinement effects on translational mobility are important for $\Psi(t)$ relaxation. Note that the pore anisotropy effects on the RR and $\Delta\Delta$ components are in opposite directions, so that the difference between the total $\Psi_{a-\rho}(t)$ and $\Psi_{xy}(t)$ is smaller than that for the corresponding RR and $\Delta\Delta$ components.

Even though orientational relaxation accounts for only a portion of the relaxation mechanism of $\Psi(t)$ for confined liquid acetonitrile, it does play an important role. It is thus of interest to also examine to what extent the collective reorientation contributing to OKE differs from single-molecule reorientation.

Using eq 6, the collective orientational TCF can be rewritten as

$$\begin{aligned}\Psi^{\text{MM}}(t) &= \frac{15}{N} \sum_{i=1}^N \sum_{j=1}^N \langle Q_{i,xz}(0)Q_{j,xz}(t) \rangle \\ &= \Psi^{\text{MMs}}(t) + \Psi^{\text{MMP}}(t)\end{aligned}\quad (26)$$

It is a sum of single-molecule and pair terms $\Psi^{\text{MMs}}(t)$ and $\Psi^{\text{MMP}}(t)$. Its single-molecule portion is

$$\Psi^{\text{MMs}}(t) = \frac{15}{N} \sum_{i=1}^N \langle Q_{i,xz}(0)Q_{i,xz}(t) \rangle \quad (27)$$

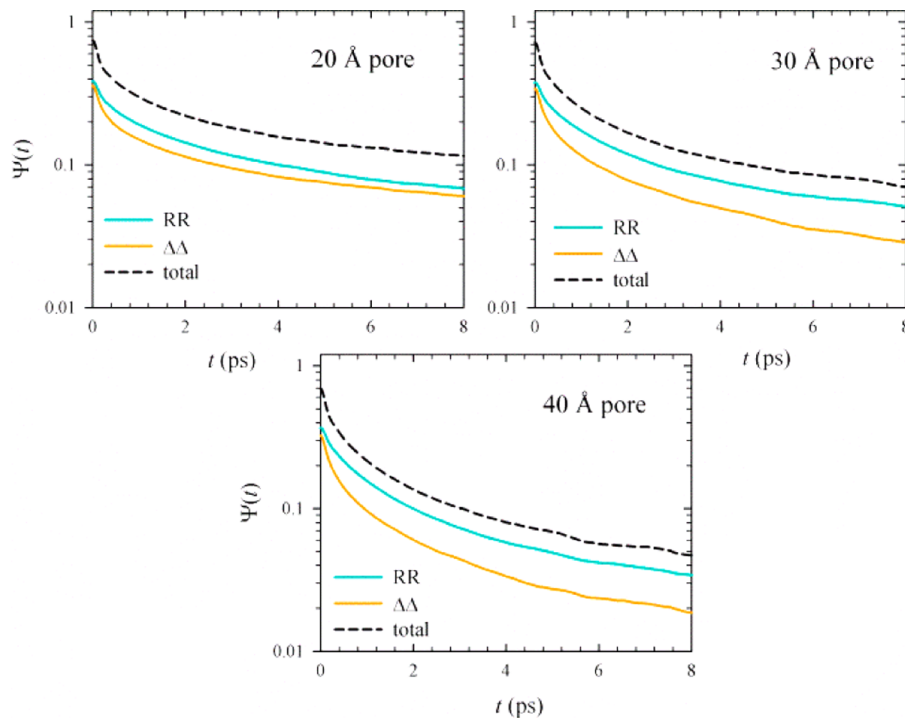


Figure 11. Polarizability anisotropy time correlation $\Psi(t)$ and its rotational relaxation and collision-induced components $\Psi^{RR}(t)$ and $\Psi^{\Delta\Delta}(t)$ for acetonitrile in silica pore of diameters 20, 30, and 40 Å.

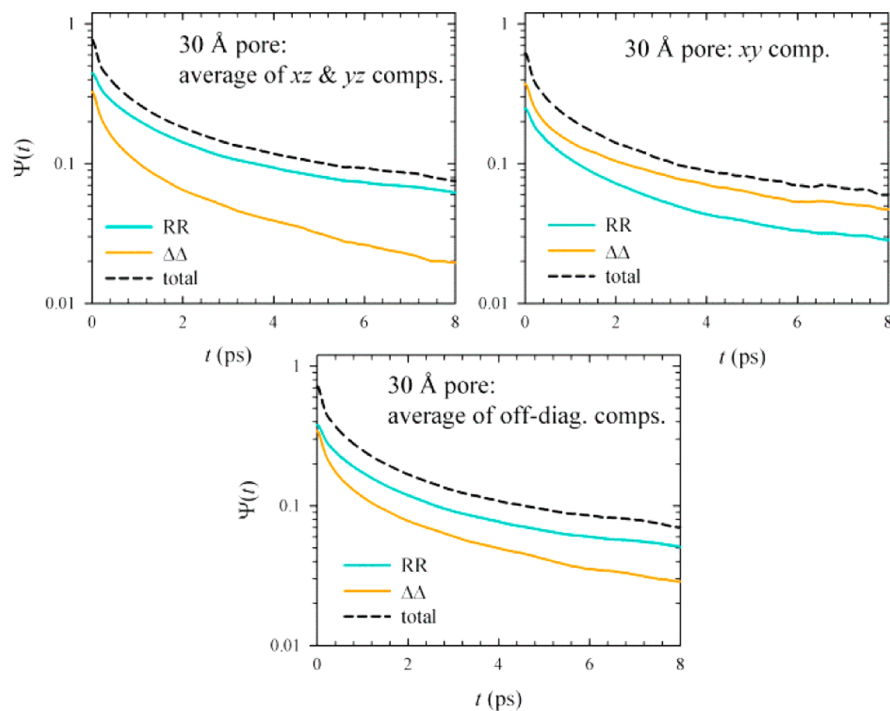


Figure 12. Relaxation of off-diagonal components of anisotropic polarizability in a 30 Å diameter cylindrical pore with axis along z . The top left panel displays $[\Psi_{xz}(t) + \Psi_{yz}(t)]/2$, top right panel $\Psi_{xy}(t)$, and the bottom panel the average $[\Psi_{xy}(t) + \Psi_{xz}(t) + \Psi_{yz}(t)]/3$ over the three components. In every panel, the total TCF and its RR, and $\Delta\Delta$ components are shown.

In Figure 13 are displayed $\Psi^{MM_s}(t)$ and $\Psi^{MM}(t)$ for acetonitrile in silica pores, calculated using all off-diagonal components of the second-rank orientational tensor \mathbf{Q}_s .

As can be seen from the Figure, in all cases $\Psi^{MM_s}(t)$ decays slightly faster than $\Psi^{MM}(t)$ for the first 2 ps, but then decays more slowly at long times. This indicates that anticorrelation of pairs of

molecules is significant on the longer time scale, giving rise to a negative $\Psi^{MM_p}(t)$.

3.C. Optical Kerr Effect Nuclear Response and Comparison with Experiment. The OKE nuclear response $R^{nuc}(t)$ can be obtained by differentiating $\Psi(t)$, as is shown in eq 22. Numerical differentiation provides reasonable results at short

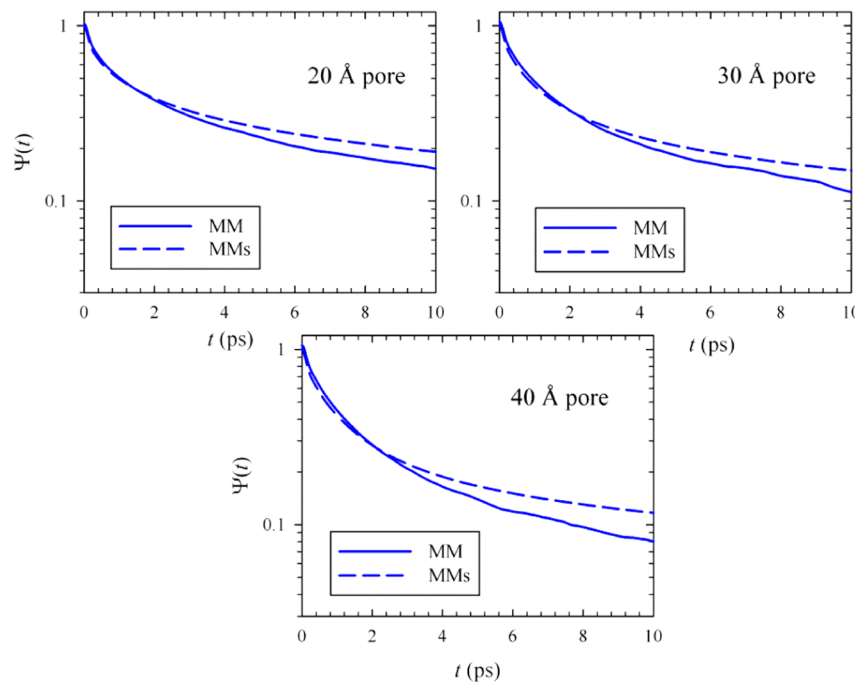


Figure 13. Single-molecule and collective orientational TCFs $\Psi^{MMs}(t)$ and $\Psi^{MM}(t)$ for acetonitrile in silica pores.

times, but it amplifies noise present in $\Psi(t)$ and is therefore less useful as slow decay sets in at longer times. To obtain results at longer times that are not marred by noise, we fit $\Psi(t)$ and differentiate the fitting functions to compare our results with experiments³ that have been analyzed by fitting the OKE response for $t > 5$ ps to sums of exponentials.^{3,12}

We display our results and their comparison to experiment in Figure 14. The top panel shows the short-time portion of $R^{nuc}(t)$, calculated as $-\dot{\Psi}(t)/\Psi(0)$ by numerical differentiation. The peak in $R^{nuc}(t)$ arises from the nondiffusive portion of the nuclear response, including librational contributions to rotational dynamics. Our results indicate that this peak is more pronounced for the bulk than for confined acetonitrile, which is consistent with the expectation that the confined liquid is subject to stronger forces and torques. In all four systems the subsequent decay includes a shoulder before the diffusive portion sets in.

Experiments have focused on the analysis of the decay of $R^{nuc}(t)$ that occurs beyond the 2 ps scale displayed in the top panel of Figure 14. In bulk acetonitrile, this portion of the response is well-represented as a single exponential decay:^{3,12,16}

$$R_{\text{bulk}}^{\text{fit}}(t) \propto \exp(-t/\tau_1) \quad (28)$$

To fit the corresponding portion of the response in confined acetonitrile, Loughnane et al.³ included two additional exponential decays with relaxation times τ_2 and τ_3 independent of the pore diameter:

$$R_{\text{pore}}^{\text{fit}}(t) = A_1 \exp(-t/\tau_1) + A_2 \exp(-t/\tau_2) + A_3 \exp(-t/\tau_3) \quad (29)$$

In fitting our data, we have taken a similar approach in that we have assumed that τ_1 is the same for acetonitrile bulk and confined liquid and that the times τ_2 and τ_3 are the same for all three pores. However, our fits were carried out on $\Psi(t)$, for which the slowly decaying portions have a larger amplitude than in the case of $R^{nuc}(t)$. The portion of $\Psi(t)$ that corresponds to exponential decays is differentiated to obtain $R^{\text{fit}}(t)$. The

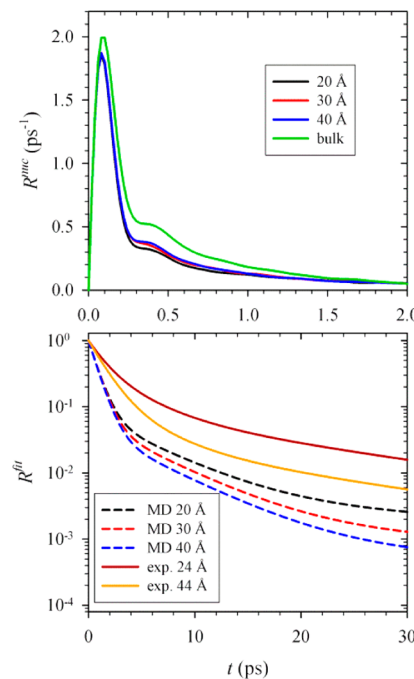


Figure 14. Top panel: Short-time OKE nuclear response calculated by numerical differentiation of $\Psi(t)$. Shown are the MD results for acetonitrile in the three pores and in bulk liquid. Bottom panel: OKE response from the fits to data at longer times. The MD data, obtained by differentiating the fit to longer-time portion of $\Psi(t)$ for confined acetonitrile, are compared to the corresponding fits to the experimental OKE response.³ Experimental results at 309 K are shown.

resulting parameters for normalized $R^{\text{fit}}(t)$ are given in Table 3, and comparison with experiment is displayed in the bottom panel of Figure 14. As can be seen from the Figure, our results agree well with experiment at longer times (>6 ps) but exhibit short-time decay that is too fast, consistent with the fact that our τ_1 is significantly shorter than the experimental value of 1.4 ps.^{3,16}

Table 3. Fit Parameters for Normalized Long-Time OKE Response

system	A_1	τ_1 (ps)	A_2	τ_2 (ps)	$A_3 = 1 - A_1 - A_2$	τ_3 (ps)
20 Å diam.	0.954	0.819	0.072	5.31	0.004	56.5
30 Å diam.	0.941		0.057		0.002	
40 Å diam.	0.954		0.045		0.001	

This problem may be partially due to the three-site acetonitrile model that we have used, which tends to overestimate somewhat the molecular orientational relaxation rate.⁵⁰ We find that the exponential decay time associated with $C_2(t)$ at 300 K is 0.91 ps, while corresponding time³¹ for the six-site model of Böhm et al. is 1.15 ps.⁶⁴ A more recent six-site model of Nikitin and Lyubartsev⁶⁵ leads to a bulk τ_1 value of 1.39 ps,³¹ in good agreement with experiment. We expect that improved agreement for OKE in nanopores would result from the use of a similar all-atom representation of acetonitrile.

4. SUMMARY AND CONCLUSIONS

We have reported our MD simulation results for polarizability anisotropy relaxation of liquid acetonitrile in approximately cylindrical silica pores of diameters ranging from 20 to 40 Å and compared them with polarizability anisotropy relaxation of bulk liquid acetonitrile. Our results are consistent with the OKE experiments carried out for acetonitrile in silica pores of similar dimensions and can be well represented using the same type of data analysis.^{3,12}

We included the contributions of molecular and interaction-induced polarizabilities in our model for the polarizability anisotropy TCF $\Psi(t)$ and determined how these components contribute to the observed relaxation. To gain deeper understanding of the structure and dynamics of acetonitrile in silica pores, we also determined several structural parameters and measures of single-molecule rotational and translational mobility in interfacial layers. We summarize here our main findings.

The polarizability anisotropy TCF for acetonitrile in silica pores decays nonexponentially, with a slowly decaying component that has a similar decay rate in pores of different diameter but has a larger amplitude in smaller pores.

This behavior is related to the fact that translational MSDs and single-molecule orientational TCFs exhibit pronounced slowdown in layers close to the silica surface. In the pore diameter range we studied, the reduction in molecular mobility in these regions is primarily a function of the distance from the interface. It should be noted that slow relaxation of acetonitrile at a flat silica interface has been shown by MD to influence long-time relaxation $\Psi(t)$ in a liquid acetonitrile film,³¹ although the reduction in mobility was less dramatic than that in the present nanopore case.

Using a projection scheme that identifies the total intensity of the contribution to $\Psi(t)$ from collective reorientation, we found that this contribution, $\Psi^{RR}(t)$, and the contribution from the “collision-induced” polarizability anisotropy, $\Psi^{\Delta\Delta}(t)$, are weakly coupled, with their cross-correlation $\Psi^{R\Delta}(t)$ small and more rapidly decaying than the two autocorrelations. $\Psi^{RR}(t)$ and $\Psi^{\Delta\Delta}(t)$ both include a slowly decaying portion, which has a somewhat larger amplitude for $\Psi^{RR}(t)$ than for $\Psi^{\Delta\Delta}(t)$, indicating that slow collective reorientation plays a somewhat more important role at long times than slow translational dynamics contributing to $\Psi^{\Delta\Delta}(t)$.

We have examined how pore anisotropy might influence the relaxation processes observed by OKE. In addition to calculating $\Psi(t)$ as an average over all off-diagonal components, we have

compared its contributions from axial-radial components $\Psi_{a-\rho}(t) = [\Psi_{xz}(t) + \Psi_{yz}(t)]/2$, where z is the pore axis, with the purely radial $\Psi_{xy}(t)$. We found that these effects are quite large, affecting the relative magnitudes and relaxation rates of $\Psi^{RR}(t)$ and $\Psi^{\Delta\Delta}(t)$.

We have also examined how much the collective and single-molecule orientational TCFs, $\Psi^{MM}(t)$ and $\Psi^{MMS}(t)$, contributing to polarizability anisotropy relaxation in the pores, differ. We found that at long times $\Psi^{MM}(t)$ decays faster than $\Psi^{MMS}(t)$, indicating that anticorrelated molecular pairs in interfacial layers influence long-time collective reorientation.

Our work indicates that understanding and analyzing the effects of confinement on collective TCFs, such as $\Psi(t)$, presents new challenges beyond those present for single-molecule relaxation. We are continuing this work by extending our investigation of polarizability anisotropy relaxation to other confined liquids. We are also focusing on the use of improved potential models that would lead to closer quantitative agreement with experiment.

■ ASSOCIATED CONTENT

S Supporting Information

Included are the results for mean-squared displacements and orientational time correlations for acetonitrile molecules residing continuously in three interfacial shells of silica pores. Also included is information on the fitting procedure and parameters for the polarizability anisotropy time correlations. This material is available free of charge via the Internet at <http://pubs.acs.org>.

■ AUTHOR INFORMATION

Corresponding Authors

*E-mail: anatoli.milischuk@gmail.com.

*Phone: +1 970 491 5196. E-mail: Branka.Ladanyi@colostate.edu.

Notes

The authors declare no competing financial interest.

■ ACKNOWLEDGMENTS

This work was partially supported by the National Science Foundation (NSF) Grant Nos. CHE 0911668 and 1213682. We are grateful to Profs. Ward H. Thompson and John T. Fourkas for helpful discussions.

■ REFERENCES

- (1) Farrer, R. A.; Fourkas, J. T. Orientational Dynamics of Liquids Confined in Nanoporous Sol-Gel Glasses Studied by Optical Kerr Effect Spectroscopy. *Acc. Chem. Res.* **2003**, *36*, 605–612.
- (2) Farrer, R. A.; Loughnane, B. J.; Fourkas, J. T. Dynamics of Confined Carbon Disulfide from 165 to 310 K. *J. Phys. Chem. A* **1997**, *101*, 4005–4010.
- (3) Loughnane, B. J.; Farrer, R. A.; Scodinu, A.; Fourkas, J. T. Dynamics of a Wetting Liquid in Nanopores: An Optical Kerr Effect Study of the Dynamics of Acetonitrile Confined in Sol-Gel Glasses. *J. Chem. Phys.* **1999**, *111*, 5116–5123.
- (4) Loughnane, B. J.; Farrer, R. A.; Scodinu, A.; Reilly, T.; Fourkas, J. T. Ultrafast Spectroscopic Studies of the Dynamics of Liquids Confined in Nanoporous Glasses. *J. Phys. Chem. B* **2000**, *104*, 5421–5429.

- (5) Loughnane, B. J.; Fourkas, J. T. Geometric Effects in the Dynamics of a Nonwetting Liquid in Microconfinement: An Optical Kerr Effect Study of Methyl Iodide in Nanoporous Glasses. *J. Phys. Chem. B* **1998**, *102*, 10288–10294.
- (6) Loughnane, B. J.; Scodinu, A.; Fourkas, J. T. Extremely Slow Dynamics of a Weakly Wetting Liquid at a Solid/Liquid Interface: CS₂ Confined in Nanoporous Glasses. *J. Phys. Chem. B* **1999**, *103*, 6061–6068.
- (7) Loughnane, B. J.; Scodinu, A.; Fourkas, J. T. Temperature-Dependent Optical Kerr Effect Spectroscopy of Chloroform in Restricted Geometries. *Chem. Phys.* **2000**, *253*, 323–330.
- (8) Scodinu, A.; Fourkas, J. T. Comparison of the Orientational Dynamics of Water Confined in Hydrophobic and Hydrophilic Nanopores. *J. Phys. Chem. B* **2002**, *106*, 10292–10295.
- (9) Ratajska-Gadomska, B.; Bialkowski, B.; Gadomski, W.; Radzewicz, C.: Ultrafast Optical Kerr Effect Spectroscopy of Water Confined in Nanopores of the Gelatin Gel. *J. Chem. Phys.* **2007**, *126*.
- (10) Tortschanoff, A.; Campa, E. P.; van Mourik, F.; Chergui, M. Optical Kerr Effect Studies of the Dynamics of Confined Water. *Microelectron. J.* **2008**, *39*, 1257–1258.
- (11) Schwalb, G.; Deeg, F. W.; Bräuchle, C. Influence of Surface Interaction on the Reorientational Dynamics of Pentylcyanobiphenyl Confined in a Porous Glass. *J. Non-Cryst. Solids* **1994**, *172*–174 (Part 1), 348–352.
- (12) Loughnane, B. J.; Farrer, R. A.; Fourkas, J. T. Evidence for the Direct Observation of Molecular Exchange of a Liquid at the Solid/Liquid Interface. *J. Phys. Chem. B* **1998**, *102*, 5409–5412.
- (13) Smith, N. A.; Meech, S. R. Optically-Heterodyne-Detected Optical Kerr Effect (OHD-OKE): Applications in Condensed Phase Dynamics. *Int. Rev. Phys. Chem.* **2002**, *21*, 75–100.
- (14) Zhong, Q.; Fourkas, J. T. Optical Kerr Effect Spectroscopy of Simple Liquids. *J. Phys. Chem. B* **2008**, *112*, 15529–15539.
- (15) McMorrow, D. Separation of Nuclear and Electronic Contributions to Femtosecond 4-Wave-Mixing Data. *Opt. Commun.* **1991**, *86*, 236–244.
- (16) McMorrow, D.; Lotshaw, W. T. Intermolecular Dynamics in Acetonitrile Probed with Femtosecond Fourier-Transform Raman Spectroscopy. *J. Phys. Chem.* **1991**, *95*, 10395–406.
- (17) Luo, R. S.; Jonas, J. Raman Scattering Study of Liquid Ethylene Glycol Confined to Nanoporous Silica Glasses. *J. Raman Spectrosc.* **2001**, *32*, 975–978.
- (18) Hiramara, Y.; Takahashi, T.; Hino, M.; Sato, T. Studies of Water Adsorbed in Porous Vycor Glass. *J. Colloid Interface Sci.* **1996**, *184*, 349–359.
- (19) Anwander, R.; Nagl, I.; Widenmeyer, M.; Engelhardt, G.; Groeger, O.; Palm, C.; Roser, T. Surface Characterization and Functionalization of MCM-41 Silicas Via Silazane Silylation. *J. Phys. Chem. B* **2000**, *104*, 3532–3544.
- (20) Grate, J. W.; Dehoff, K. J.; Warner, M. G.; Pittman, J. W.; Wietsma, T. W.; Zhang, C. Y.; Oostrom, M. Correlation of Oil-Water and Air-Water Contact Angles of Diverse Silanized Surfaces and Relationship to Fluid Interfacial Tensions. *Langmuir* **2012**, *28*, 7182–7188.
- (21) Cang, H.; Novikov, V. N.; Fayer, M. D. Experimental Observation of a Nearly Logarithmic Decay of the Orientational Correlation Function in Supercooled Liquids on the Picosecond-to-Nanosecond Time Scales. *Phys. Rev. Lett.* **2003**, *90*, 197401.
- (22) Cang, H.; Novikov, V. N.; Fayer, M. D. Logarithmic Decay of the Orientational Correlation Function in Supercooled Liquids on the ps to ns Time Scale. *J. Chem. Phys.* **2003**, *118*, 2800–2807.
- (23) Kruk, M.; Jaroniec, M.; Sayari, A. Adsorption Study of Surface and Structural Properties of MCM-41 Materials of Different Pore Sizes. *J. Phys. Chem. B* **1997**, *101*, 583–589.
- (24) Gulmen, T. S.; Thompson, W. H. Grand Canonical Monte Carlo Simulations of Acetonitrile Filling of Silica Pores of Varying Hydrophilicity/Hydrophobicity. *Langmuir* **2009**, *25*, 1103–1111.
- (25) Cheng, L. W.; Morrone, J. A.; Berne, B. J. Structure and Dynamics of Acetonitrile Confined in a Silica Nanopore. *J. Phys. Chem. C* **2012**, *116*, 9582–9593.
- (26) Morales, C. M.; Thompson, W. H. Simulations of Infrared Spectra of Nanoconfined Liquids: Acetonitrile Confined in Nanoscale, Hydrophilic Silica Pores. *J. Phys. Chem. A* **2009**, *113*, 1922–1933.
- (27) Ladanyi, B. M.; Liang, Y. Q. Interaction-Induced Contributions to Polarizability Anisotropy Relaxation in Polar Liquids. *J. Chem. Phys.* **1995**, *103*, 6325–32.
- (28) Ladanyi, B. M.; Skaf, M. S.; Liang, Y. Q. Interaction-Induced Contributions to Spectra of Polar Liquids. In *Collision- and Interaction-Induced Spectroscopy*; Tabisz, G. C., Neuman, M. N., Eds.; Kluwer: Dordrecht, The Netherlands, 1995; Vol. 452, pp 143–57.
- (29) Elola, M. D.; Ladanyi, B. M. Polarizability Response in Polar Solvents: Molecular-Dynamics Simulations of Acetonitrile and Chloroform. *J. Chem. Phys.* **2005**, *122*, 224506.
- (30) Ladanyi, B. M.; Klein, S. Contributions of Rotation and Translation to Polarizability Anisotropy and Solvation Dynamics in Acetonitrile. *J. Chem. Phys.* **1996**, *105*, 1552–1561.
- (31) Hu, Z. H.; Weeks, J. D. Acetonitrile on Silica Surfaces and at Its Liquid-Vapor Interface: Structural Correlations and Collective Dynamics. *J. Phys. Chem. C* **2010**, *114*, 10202–10211.
- (32) Madden, P. A. Interaction-Induced Phenomena. In *Molecular Liquids: Dynamics and Interactions*; Barnes, A. J., Orville-Thomas, W. J., Yarwood, J., Eds.; Reidel: Dordrecht, The Netherlands, 1984; pp 431–74.
- (33) Madden, P. A.; Tildesley, D. J. Interaction-Induced Contributions to Rayleigh and Allowed Raman Bands - a Simulation Study of CS₂. *Mol. Phys.* **1985**, *55*, 969–998.
- (34) Ladanyi, B. M. Molecular Dynamics Study of Rayleigh Light Scattering from Molecular Fluids. *J. Chem. Phys.* **1983**, *78*, 2189–203.
- (35) Frenkel, D.; McTague, J. P. Molecular-Dynamics Studies of Orientational and Collision- Induced Light-Scattering in Molecular Fluids. *J. Chem. Phys.* **1980**, *72*, 2801–2818.
- (36) Berne, B. J.; Pecora, R. *Dynamic Light Scattering: With Applications to Chemistry, Biology, and Physics*; Wiley-Interscience: New York, 1975.
- (37) Keyes, T.; Ladanyi, B. M. The Internal Field Problem in Depolarized Light Scattering. *Adv. Chem. Phys.* **1984**, *56*, 411–65.
- (38) Gulmen, T. S.; Thompson, W. H. Model Silica Pores with Controllable Surface Chemistry for Molecular Dynamics Simulations. *MRS Online Proc. Libr.* **2005**, *899*, 10.1557/PROC-0899-N06-05.
- (39) Gulmen, T. S.; Thompson, W. H. Testing a Two-State Model of Nanoconfined Liquids: Conformational Equilibrium of Ethylene Glycol in Amorphous Silica Pores. *Langmuir* **2006**, *22*, 10919–10923.
- (40) Milischuk, A. A.; Ladanyi, B. M. Structure and Dynamics of Water Confined in Silica Nanopores. *J. Chem. Phys.* **2011**, *135*, 174709.
- (41) Milischuk, A. A.; Krewald, V.; Ladanyi, B. M. Water Dynamics in Silica Nanopores: The Self-Intermediate Scattering Functions. *J. Chem. Phys.* **2012**, *136*, 224704.
- (42) Martin, M. G.; Chen, B.; Wick, C. D.; Potoff, J. J.; Stubbs, J. M.; Siepmann, J. I. *Mcccs Towhee*; <http://towhee.sourceforge.net>.
- (43) Martin, M. G.; Siepmann, J. I. Novel Configurational-Bias Monte Carlo Method for Branched Molecules. Transferable Potentials for Phase Equilibria. 2. United-Atom Description of Branched Alkanes. *J. Phys. Chem. B* **1999**, *103*, 4508–4517.
- (44) Smith, W.; Todorov, I. T. A Short Description of Dl_Poly. *Mol. Simul.* **2006**, *32*, 935–943.
- (45) Nosé, S. A Unified Formulation of the Constant-Temperature Molecular-Dynamics Methods. *J. Chem. Phys.* **1984**, *81*, 511–519.
- (46) Nosé, S. A Molecular Dynamics Method for Simulations in the Canonical Ensemble. *Mol. Phys.* **1984**, *52*, 255–268.
- (47) Hoover, W. G. Canonical Dynamics - Equilibrium Phase-Space Distributions. *Phys. Rev. A* **1985**, *31*, 1695–1697.
- (48) Darden, T.; York, D.; Pedersen, L. Particle Mesh Ewald: An N-Log(N) Method for Ewald Sums in Large Systems. *J. Chem. Phys.* **1993**, *98*, 10089–10092.
- (49) Allen, M. P.; Tildesley, D. J. *Computer Simulation of Liquids*; Oxford University Press: New York, 1987.
- (50) Gee, P. J.; Van Gunsteren, W. F. Acetonitrile Revisited: A Molecular Dynamics Study of the Liquid Phase. *Mol. Phys.* **2006**, *104*, 477–483.

- (51) Bródka, A.; Zerda, T. W. Properties of Liquid Acetone in Silica Pores: Molecular Dynamics Simulation. *J. Chem. Phys.* **1996**, *104*, 6319–6326.
- (52) Burnham, A. K.; Alms, G. R.; Flygare, W. H. The Local Electric Field. I. The Effect on Isotropic and Anisotropic Rayleigh Scattering. *J. Chem. Phys.* **1975**, *62*, 3289–3297.
- (53) Brovchenko, I.; Geiger, A.; Oleinikova, A. Water in Nanopores. I. Coexistence Curves from Gibbs Ensemble Monte Carlo Simulations. *J. Chem. Phys.* **2004**, *120*, 1958–1972.
- (54) Ding, F.; Hu, Z.; Zhong, Q.; Manfred, K.; Gattass, R. R.; Brindza, M. R.; Fourkas, J. T.; Walker, R. A.; Weeks, J. D. Interfacial Organization of Acetonitrile: Simulation and Experiment. *J. Phys. Chem. C* **2010**, *114*, 17651–17659.
- (55) Mancinelli, R.; Imberti, S.; Soper, A. K.; Liu, K. H.; Mou, C. Y.; Bruni, F.; Ricci, M. A. Multiscale Approach to the Structural Study of Water Confined in Mcm41. *J. Phys. Chem. B* **2009**, *113*, 16169–16177.
- (56) Brodka, A. Diffusion in Restricted Volume. *Mol. Phys.* **1994**, *82*, 1075–1078.
- (57) Mittal, J.; Truskett, T. M.; Errington, J. R.; Hummer, G.: Layering and Position-Dependent Diffusive Dynamics of Confined Fluids. *Phys. Rev. Lett.* **2008**, *100*.
- (58) Brovchenko, I.; Geiger, A.; Oleinikova, A.; Paschek, D. Phase Coexistence and Dynamic Properties of Water in Nanopores. *Eur. Phys. J. E* **2003**, *12*, 69–76.
- (59) Liu, P.; Harder, E.; Berne, B. J. On the Calculation of Diffusion Coefficients in Confined Fluids and Interfaces with an Application to the Liquid-Vapor Interface of Water. *J. Phys. Chem. B* **2004**, *108*, 6595–6602.
- (60) Laage, D.; Thompson, W. H. Reorientation Dynamics of Nanoconfined Water: Power-Law Decay, Hydrogen-Bond Jumps, and Test of a Two-State Model. *J. Chem. Phys.* **2012**, *136*, 044513.
- (61) Chowdhary, J.; Ladanyi, B. M. Molecular Simulation Study of Water Mobility in Aerosol-Ot Reverse Micelles. *J. Phys. Chem. A* **2011**, *115*, 6306–6316.
- (62) Pinnick, E. R.; Erramilli, S.; Wang, F. Computational Investigation of Lipid Hydration Water of L-Alpha 1-Palmitoyl-2-Oleoyl-Sn-Glycerol-3-Phosphocholine at Three Hydration Levels. *Mol. Phys.* **2010**, *108*, 2027–2036.
- (63) Scodinu, A.; Farrer, R. A.; Fourkas, J. T. Direct Observation of Different Mechanisms for the Inhibition of Molecular Reorientation at a Solid/Liquid Interface. *J. Phys. Chem. B* **2002**, *106*, 12863–12865.
- (64) Böhm, H. J.; Lynden-Bell, R. M.; Madden, P. A.; McDonald, I. R. Molecular Motion in a Model of Liquid Acetonitrile. *Mol. Phys.* **1984**, *51*, 761–777.
- (65) Nikitin, A. M.; Lyubartsev, A. P. New Six-Site Acetonitrile Model for Simulations of Liquid Acetonitrile and Its Aqueous Mixtures. *J. Comput. Chem.* **2007**, *28*, 2020–2026.